In Vivo Prostate Magnetic Resonance Imaging and Magnetic Resonance Spectroscopy at 3 Tesla Using a Transceive Pelvic Phased Array Coil

Preliminary Results

Hee-Won Kim, PhD,§ David L. Buckley, PhD,†§ David M. Peterson, MS,* G. Randy Duensing, PhD,‡¶ Jim Caserta, MS,* Jeffrey Fitzsimmons, PhD,* and Stephen J. Blackband, PhD,†§‖*

Abstract: Magnetic resonance (MR) systems operating at 3 Telsa (T) and above have demonstrated considerable potential in human studies, offering improved signal-to-noise ratio and spectral resolution. However, because of radiofrequency limitations and concerns, and the lack of large volume body coils, most studies have been limited to the head. In this study we describe the design and construction of a transceive pelvic phased array coil with which MR images and spectra of the human prostate at 3 T have been obtained. Comparison with 1.5 T instruments with different hardware configurations is difficult; however, in a preliminary comparison the signal-to-noise ratio is improved in phantoms and humans when compared with a 1.5 T receive-only pelvic phased array coil, and high quality spectral resolution is demonstrated through the delineation of the citrate quadruplet in localized ^{1}H prostate spectra. Higher fields offer the potential for MR prostate studies without the use of an endorectal coil.

From the *Departments of Radiology, †Neuroscience and ‡Electrical and Computer Engineering, and the §UF Brain Institute, University of Florida, Gainesville, FL; ¶MRI Devices Corp., Gainesville, FL; and the ‖National High Magnetic Field Laboratory, Tallahassee, FL.

Presented at the 7th Annual Meeting of ISMRM in Philadelphia, Pennsylvania, May 1999.

Received August 2, 2002, and accepted for publication, after revision, November 19, 2002.

Supported by University of Florida McKnight Brain Institute, the National High Magnetic Field Laboratory, and grant funding from the NIH (R01 DK51014, R01 NS41094-01, and P41 RR16105).

Reprints: Hee-Won Kim, PhD, Department of Radiology, University of Florida, 1600 SW Archer Rd, Gainesville, FL 32610. E-mail: hwkim@ufl.edu

1521-737X/03/3807-0443

DOI: 10.1097/01.RLI.0000065425.29042.8d

Key Words: transceive, phased-array, high field, 3.0 Tesla, prostate, MRI, MRS

(*Invest Radiol* 2003;38: 443–451)

Magnetic resonance imaging (MRI) and spectroscopy of the pathologic prostate gland have shown considerable potential in determining the stage of the disease, differentiating benign prostatic hyperplasia from carcinoma, for monitoring the course of therapy, guiding biopsy, radiation therapy treatment planning, and tumor volume measurement.[1–8] Limitation in the signal-to-noise ratio (SNR) on conventional 1.5 T clinical systems using body coils has driven the development of endorectal (ER) coils, recently used in combination with pelvic phased array (PPA) coils.[9–12] This has facilitated high spatial and temporal resolution imaging and ^{1}H spectroscopy on volumes of the order of a few milliliters.[13–16] By combining the ER coil with the PPA coil, the increased SNR over the prostate offered by the ER coil is combined with the large field of view over the pelvis offered by the PPA coil.[17]

The ER coil is contraindicated in a number of patients[4] (eg, for patients examined shortly after surgery, particularly after abdominal perineal resection for rectal cancers or after radiation therapy for the pelvis). In some cases, it is better not to use an ER coil to avoid structural deformation of the prostate peripheral zone, which is often compressed by an ER coil. The ER coil also causes signal hyperintensity near the rectum and neighboring peripheral zone. The signal hyperintensity and tissue deformation can make diagnostic interpretation difficult. Ways of improving the SNR without causing tissue deformation or signal hyperintensity in the prostate are desirable.

Localized proton MR spectroscopy of the in situ human prostate is of great importance. Quantitation of citrate in the prostate can provide the means of differentiation of prostatic cancer from benign prostatic hyperplasia or normal tissue.[18] The citrate molecule contains 2 strongly coupled methylene protons. Those couplings constitute 4 peaks in the mixed state of an AB system, and it is hard to quantitate this metabolite from in vivo spectra where the peaks are not distinguished.[19]

As described above, improvements in SNR and spectral resolution are desirable in prostate studies and may potentially be achieved through the use of higher field magnets. Higher B_0 field offers improvements in spectral resolution, as well as the SNR as observed in a previous study (Fitzsimmons JR et al., Abstract ISMRM, 1997; p.174). Since the 3 T (and higher field) whole body system was developed, most studies have been applied to the central nervous system on these magnets. Few studies have examined the application of high-field MR imaging or spectroscopy to the prostate. Primarily, at higher B_0 field strength the penetration of radiofrequency (RF) field of higher frequency into the electrically conductive body tissue is decreased. Another limitation of high fields for prostate studies is that RF power deposition in the body increases as B_0^2.[20] RF coil construction for high fields is also limited by the difficulties in tuning large coils to higher frequencies and in achieving sufficient transmitting power.

Prostate imaging is commonly performed using the body coil as a transceiver, with the body coil transmitting and a receive-only PPA, or with the body coil transmitting and a PPA/ER receiver coil combination in 1.5 T clinical system. Recently, 3 T instruments with body coils have emerged. Yet applications in the pelvic region are restricted because of the problems of high power demand and power deposition.

In this preliminary study, we developed a transceive phased array coil and demonstrated the feasibility of prostate examinations at 3 T using this coil assembly. As an alternative to a body coil at 3 T, the transceive phased array coil can alleviate major problems in construction of large volume coils and excessive RF power deposition as has been demonstrated at 3 T for studies of the spine using a transceive phased array (Duensing GR et al., Abstract ISMRM. 1998; p. 441). The transceive phased array offers reduced power requirements, SNR improvement and easier construction than large volume coils at higher frequencies. A transceive RF coil assembly was devised and built specifically for MR studies of the prostate (although it may have utility throughout the pelvis). We adopted a surface coil approach to improve the SNR. The coil consists of 2 sets of quadrature surface coils combined by an array T/R switch. To distinguish it from the conventional receive only PPA coil, the coil is referred to as a transceive PPA (TPPA; Kim H-W et al., Abstract ISMRM. 1999; p.116). The utility of the TPPA coil for prostate MRI and MRS was tested on several normal volunteers.

MATERIALS AND METHODS

Because the prostate is situated in the middle of the pelvis, 2 sets of transceiver probes facing each other, anterior and posterior, are combined to generate a B_1 field over the prostate and receive the signal from it effectively. The transmission was driven in quadrature mode to reduce the power necessary for a given flip angle and to make the excitation more uniform.[21] The 2 quadrature sets, anterior and posterior, were then combined as a 4-channel receiver in phased-array mode.[22]

Each quadrature coil was built on concave frames. All coil elements were made of 8 mm wide 3M™ copper strip. Two octagonal loops of dimensions 12 × 18 cm each were overlapped by approximately 3 cm where the mutual inductance was minimized. The coil's dimension was determined based upon 2 factors. First, the whole coil assembly should cover a pelvic region, including the prostate and surrounding organs. Second, a surface coil of diameter approximately equal to the depth of the signal sources of interest produces the optimum SNR achievable for detecting those signals when the sample is the dominant noise source (Edelstein WA et al., Abstract SMRM. 1985; pp. 964-965). The 2 sets of coil face each other as the subject lies on the posterior part and the anterior part is positioned on the pelvis. The distance between 2 sets ranged over 25 to 45 cm.

The capacitors were distributed at equal intervals ($\sim\lambda/10$) in a single coil elements to maintain uniform current and reduce dielectric interaction and losses from loading effects. The coils were tuned to 127.75 MHz and matched to 50 Ω with baluns using an equivalent load to that of the human body. Cable shield traps were employed for each coaxial line to the T/R switch to minimize cable interactions. The $\mathbf{B_1(r)}$ field produced by circular polarization from all 4 loops was simulated using the Biot–Savart law (Fig. 1). In the coronal plane, it is shown that the B_1 field is effectively produced from all 4 elements. Although the field strength diminished in the axial plane with distance from both coils, the field distribution is fairly uniform near the center of field-of-view (FOV). The phase of the current of each loop mimics the ideal current distribution at 4 points.[23] The B_1 field at the center of the FOV was enhanced when the current phase of the 4 loops was adjusted (Fig. 2).

A T/R switch was built and used with the following method to split the power to the 4 loops (Duensing GR et al., Abstract ISMRM. 1998; p. 441). The power line from the 5 kW amplifier was connected to a 2-way, zero degree splitter and then each port of this was connected to a standard quadrature splitter. Because the 4 coil elements are arranged in 2 quadrature pairs that directly face each other, the transmission was controlled so that the phases of each current were 0°, −90°, −180° and −270°. This ensures that the B_1 field in deep lying tissues such as the prostate is effectively

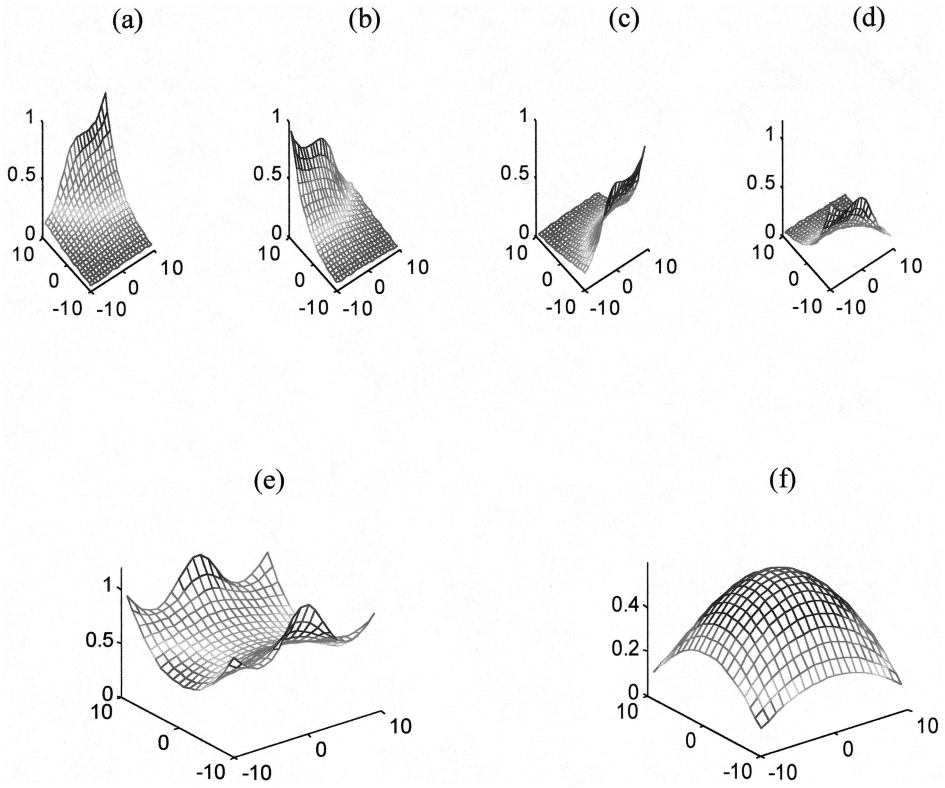

FIGURE 1. $B_1(r)$ profile of the TPPA coil where the anterior and posterior coils are 30 cm apart. The dimensions are in centimeters. The amplitude of the field is in arbitrary unit: a-e, axial plane; f, coronal plane: axial B_1 from element 1 and 2 on the anterior frame (a and b), 3 and 4 on the posterior frame (c and d). Two frames have different angles. The greater curvature of anterior frame makes the B_1 profile steeper. e, Axial B_1 profile produced by all 4 elements; f, coronal B_1 profile produced by all 4 elements.

added from the 4 coil elements as illustrated in Figure 2. Signal reception was acquired in a 4-channel phased array mode. The whole coil assembly was interfaced to a General Electric Medical Systems (Milwaukee, WI) Signa 3 T whole body MR instrument (Fig. 3).

The B_1 field and specific absorption rate (SAR) was also estimated using finite-difference time-domain simulations. The XFDTD software package from Remcom, Inc., State College, PA, was used to perform the simulations. The region was broken up into cells of size $5 \times 5 \times 5$ mm, giving a total problem size of $75 \times 75 \times 90$ cm. The body was represented by 20 different tissue types, each with the appropriate electrical parameters (conductivity σ, relative permeability ϵ_r, density ρ). Coils were modeled as thin plates of copper with width = 1 cm. The coil elements are located about 2.5 cm from the back of the human body model. Capacitors were used to tune the array elements to 128MHz. Four 1volt sinusoidal sources were used, with sources driven with the appropriate phase shifts. Time steps (20,000) of 9.6 ps were performed, yielding 24 cycles of the input signal. Circularly polarized fields are calculated using the equations: $B^+ = 0.5(B_x + iB_y)$ and $B^- = 0.5(B_x - iB_y)^*$. The B^+ within the prostate, from simulations with a 1volt source, is scaled to produce 90° and 180° flip angles. The flip angle is given by the equation $\alpha = \gamma|B^+|V\tau$, where V is the scaling factor, and τ is the length of the RF pulse. The sequence SAR can be determined using the SAR values for both 90° and 180° pulses and the details of the pulse sequence using the following equation:

$$SAR_{\text{sequence}} = \frac{N_{90}*SAR_{90}*T_{90} + N_{180}*SAR_{180}*T_{180}}{TR}$$

where N_{90} and N_{180} are the number of 90° and 180° pulses in a TR, T_{90} and T_{180} are the length, in time, of the pulses.

The performance of the 3 T TPPA coil was measured and compared with the commercial PPA General Electric (GE) coil at 1.5 T in terms of the SNR. The determination of the effectiveness of the TPPA coil compared with conventional coils is problematic because it is not feasible to operate the TPPA in receive only mode. Consequently it was decided to compare the 3 T TPPA with a PPA operating at 1.5 T because it is the goal of our study to demonstrate that the

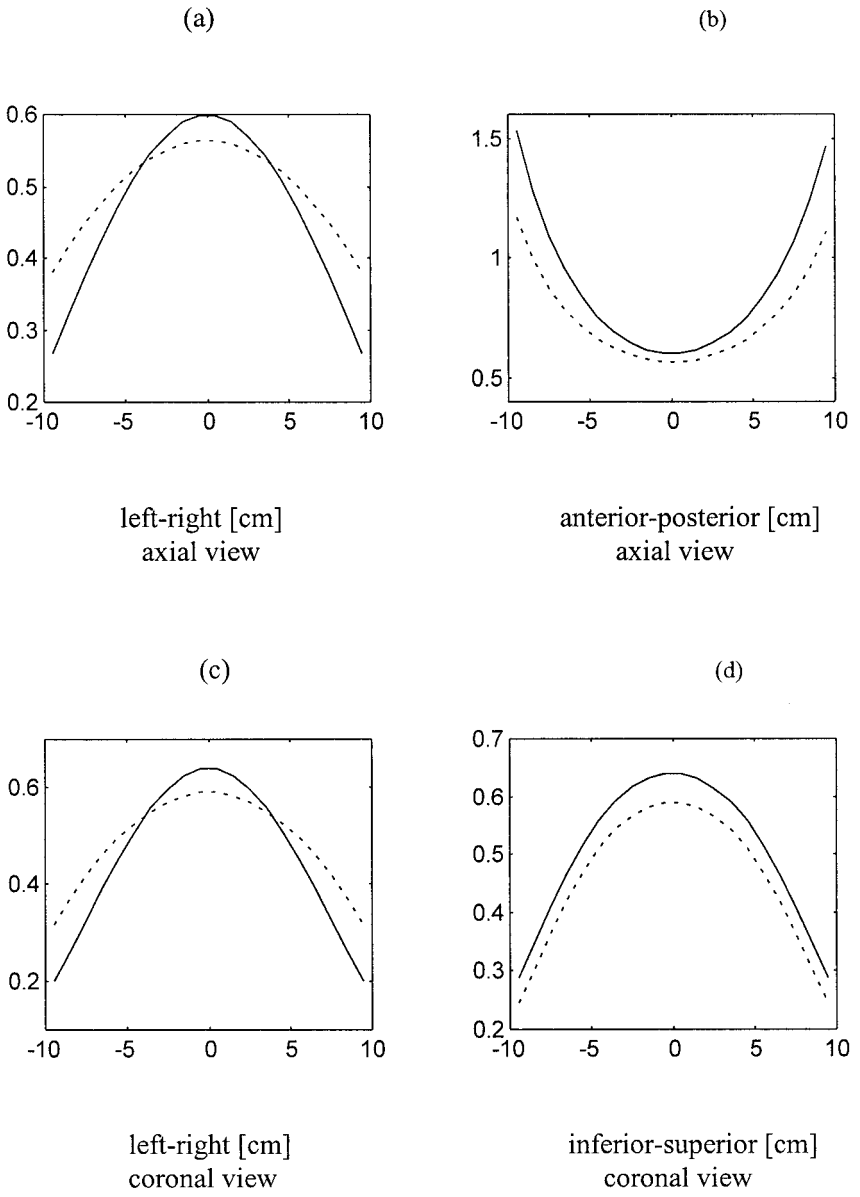

FIGURE 2. Enhanced B_1 field of the TPPA in the phased array mode (solid line) compared with linear mode (dotted line). The numbers in y-axis is arbitrary unit. Axial plane: enhanced B_1 field profile along the x-axis (left to right; a), and the y-axis (posterior to anterior; b). Coronal plane: enhanced B_1 field profile along the x-axis (left to right; c), and the z-axis (inferior to superior; d).

TPPA is as effective in terms of SNR in the prostate, and additionally offers availability of the MRS capability at high field, which provides improved spectral resolution. Even this comparison is difficult because the coil geometries are not identical, and T_1 and T_2 are different at the different field strengths. Thus to illustrate the effectiveness of the TPPA a direct comparison of 2 identical sequences at 1.5 T and 3 T was made. The SNR of TPPA coil at 3 T, transceive body coil at 1.5 T and receive-only PPA coil at 1.5 T were measured using the phantom (Model 2152220) built by GE (Milwaukee, WI). The phantom is a 2.7 L sphere containing 50 mM potassium phosphate monobasic (KH_2PO_4), 56 mM sodium hydroxide (NaOH) and 1 mL/liter Magnevist®. The coil loading of the phantom was matched to average patient and water T_1 and T_2 were reduced. Identical techniques were applied to those 2 GE Signa systems (a 1.5 T and a 3 T system, General Electric Milwaukee, USA), all using the automated GE software for prescanning (ie, setting tip angles and receiver gains). Images from the same phantom described above were acquired in the axial plane (FOV = 24 cm, matrix =

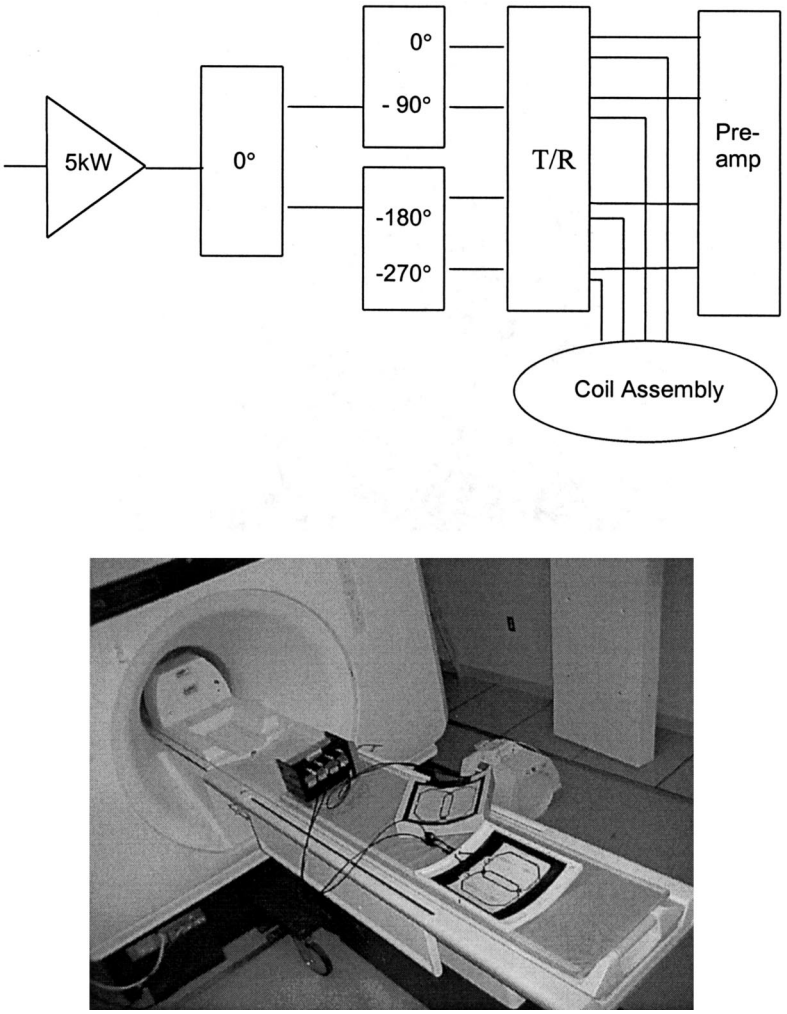

FIGURE 3. Block diagram and photograph of the 3 T pelvic phased array coil assembly.

256 × 192) using a gradient echo (GRE) sequence (TR = 500 milliseconds, TE = 15 milliseconds, flip angle = 30°), and 2 fast spin echo (FSE) sequences (TR = 2s, echo train = 2) one with a TE (effective) of 20 milliseconds and the other with a TE (effective) of 80 milliseconds. The SNR was measured in the center of the images of the phantom (approximately where the prostate would be in human studies, ROI = 757 mm^2, no. of pixels = 850).

Images were also obtained from 8 healthy volunteers (aged from 26 to 60 years). All procedures were conducted under approval from the Institutional Review Board at the University of Florida, Health Science Center and an informed consent was obtained prior to all studies. T_1- and T_2-weighted images were acquired using GRE sequence (TR=500 milliseconds, TE=8 milliseconds, flip angle=60°, FOV=24x24 cm, NEX=1.5, slice thickness=4.5mm, 256x192 matrix, acquisition time=2.28 minutes), and FSE sequence (TR=4s, TE=102 milliseconds, FOV=24x24 cm, NEX=2, echo train=8, 256x192 matrix, acquisition time=3.34 minutes), respectively.

Proton MR spectroscopy was performed using a stimulated echo acquisition mode (STEAM) sequence[24] from a 4.5 mL voxel (1.5 × 1.5 × 2 cm voxel) in the central zone of one volunteer. The STEAM parameters were: TR=1s, TE=20 milliseconds, TM=32.4 milliseconds and 512 averages.

RESULTS

It is demonstrated in Figure 4 that the entire phantom images were successfully obtained using combined 2 quadrature pairs. The signal intensity and B_1 homogeneity in the spherical phantom were enhanced by correctly controlled phases of 4 coil elements.

B^+ within the prostate region was simulated to be 0.032 μT, giving a 90° scale factor V=188. Figure 5 shows SAR results for an axial slice at the center of the array. This shows maximum absorption in the skin and muscle, due to the

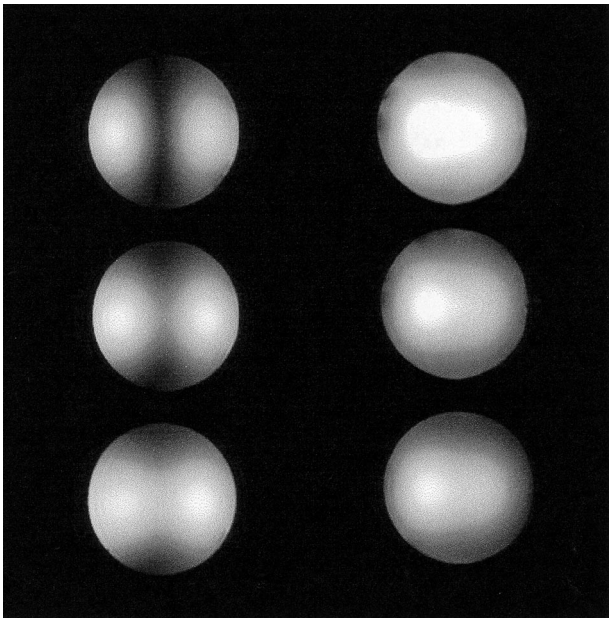

FIGURE 4. The effect of the transmitter current phases of the TPPA coil: Gradient echo images (TE=8 milliseconds, TR=500 milliseconds, flip angle = 60°) from 3 different coronal slices of the 2.7 L-sphere phantom. Slice thickness is 5 mm and 1.5 cm apart from each other. When the phases of 4 loops were set incorrectly, signal intensity fell off rapidly by depth (left). Signal was effectively enhanced where the phases of 4 loops were controlled to produce better circular polarization (right).

strength of the field in the skin and the conductivity of the muscle. Table 1 shows scaled SAR results for a multislice GRE and FSE sequences with the same scan parameters used in this study. The simulated results show that for both sequences with as many as 8 slices, the SAR is below the FDA "Non-Significant Risk Criteria" levels of 4W/kg for the whole body (15-minute average) and 8 W/kg in any gram of head or torso (5-minute average). The results are also below the normal operating mode, whole-body SAR of 1.5 W/kg specified in IEC MR Safety Standard.

TABLE 1. Simulated SAR Values

	Gradient Echo	Fast-Spin Echo
Max 1 g SAR (W/kg)	0.87	7.68
Max 10 g SAR (W/kg)	0.39	3.45
Average SAR (W/kg)	0.01	0.14
Total power (W)	2.51	15.18

The simulation shows that the SAR is below the 8W/kg in any gram of head or torso (5-minute average) for both sequences with as many as 8 slices.

The SNR from the images using TPPA at 3 T at the given ROI is 4 to 5 times higher than that using transceive body coil at 1.5 T. When compared with a 1.5 T PPA coil, the SNR was enhanced by 35% and 16% for GRE and short TE FSE, respectively, and comparable for the long TE FSE sequence as given in Table 2. The signal enhancement is not so apparent in long echo FSE as in proton density or short echo images.

High contrast-to-noise images of the prostate gland were obtained in all 8 volunteers. Examples from 2 studies are shown in Figure 6. In the T_1-weighted gradient echo image, the signal was homogeneous over the prostatic region. In T_2-weighted FSE images, it is clearly visualized that the prostate central zone and peripheral zone are differentiated with good SNR from the same volunteer (Fig. 6b and c). The contrast-to-noise ratio was sufficient to recognize a nodule in

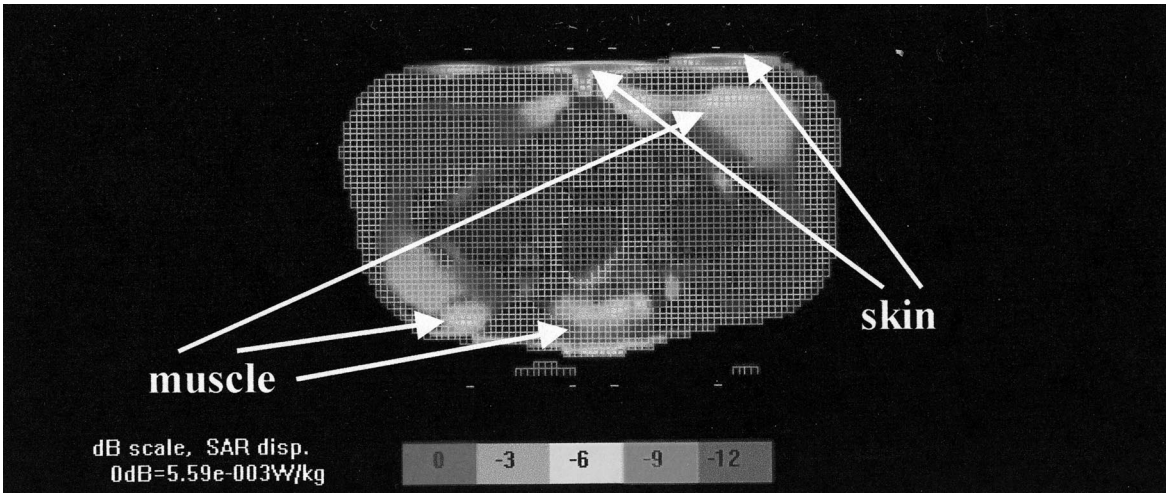

FIGURE 5. SAR map for an axial slice of the pelvis. The maximum absorption is observed in the skin and muscle, due to the strength of the field in the skin and the conductivity of the muscle.

TABLE 2. Comparison of SNR Measured in a Phantom Using the PPA at 1.5 T and the TPPA at 3.0 T

	1.5 T Body Coil	1.5 T PPA	3.0 T TPPA	SNR 3.0 T/SNR 1.5 T (body)	SNR 3.0 T/SNR 1.5 T (PPA)
GRE (15 ms/0.5 s)	43.3 ± 0.9	157.9 ± 10.0	214.0 ± 11.9	4.94	1.35
FSE (20 ms/2 s)	82.3 ± 2.2	297.1 ± 1.0	344.1 ± 6.7	4.18	1.16
FSE (80 ms/2 s)	44.7 ± 1.2	168.5 ± 6.9	169.7 ± 8.3	3.80	1.01

the central gland from these images (Fig. 6c). As predicted a higher SNR at 3 T was observed when compared with the image obtained using the body coil at 1.5 T (Fig. 6e). Figure 7 shows an example in vivo MR spectrum obtained in 8 minutes. The 4 peaks in the mixed state of an AB system from the citrate are evident and compared with a reference spectrum from a citrate phantom using the same technique.

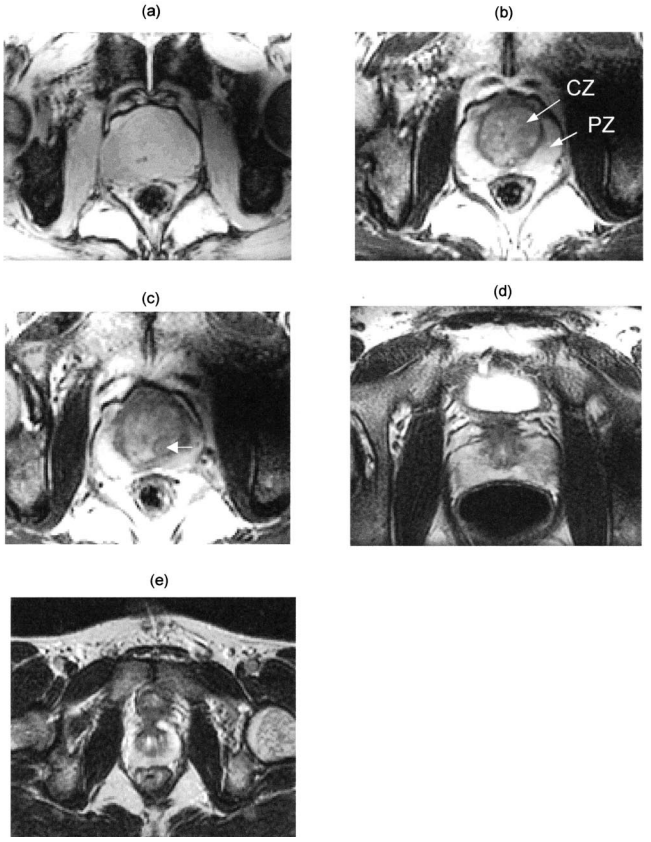

FIGURE 6. a-c, Images of a 60-year-old volunteer obtained at 3 T using the TPPA coil: a, T_1-weighted gradient echo image (TE=8 milliseconds, TR=500 milliseconds, flip angle = 60°); b and c, T_2-weighted FSE images (TE=102 milliseconds, TR=4s). The central zone (CZ) and peripheral zone (PZ) are well differentiated (b). The SNR of these images was sufficient to observe nodules in the central gland of this volunteer (c). d, T_2-weighted FSE image obtained at 3 T from a 35-year-old volunteer. E, T_2-weighted FSE image from 21-year-old volunteer using body coil at 1.5 T (TE=102 milliseconds, TR=4s).

DISCUSSION

These studies demonstrate that examination of the prostate at 3 T is feasible using a TPPA coil. Although direct comparison with external coil studies at 1.5 T[25,26] is difficult (because the coil geometry, relative FOV, and excitation/detection scheme are different), the spectral resolution of MRI and MRS at 3 T appear excellent for both phantom and human subjects and the SNR is high enough to carry out in vivo human studies.

Because T_1 at 3 T is longer than T_1 at 1.5 T, this would favor 1.5 T at the TR values used. A compromise of the TPPA is the increased RF heterogeneity arising from the array, making optimization of the SNR spatially dependent on the position within the array. Consequently, a proper comparison must also take this spatial heterogeneity into account. The SNR measured at the center of long echo T_2-weighted images acquired using the TPPA coil shows no improvement. The T_2 relaxation time at higher field is likely to be shorter than at 1.5 T and the RF characteristics of the TPPA may have further reduced the anticipated sensitivity improvement. As the FOV is defined by 4 surface coil-type TPPA elements, the signal intensity falls off more rapidly than a conventional volume coil. Moreover, when it is driven in transceive mode, the effect of the dual dependency of the signal amplitude on $(B_1)_{xy}$ is seen in more rapid fall-off of the intensity profiles with distance than that of the B_1 field profile[27] as expected in the case of the PPA coil. Furthermore, the automated prescan may not have dealt very effectively with the heterogeneous signal response of the TPPA where the magnetization profile is more like that of surface coil. Any imperfection in the 90° and 180° pulses will have compromised the SNR of the spin echo sequence. Improved prescanning protocols may be required to compensate for this response and the associated SNR shortfall. Transceive mode, however, has an SAR advantage over receive only mode where power deposition from the volume transmitter is of primary concern.

The preliminary results of ^1H spectroscopy is encouraging when compared with those previously obtained at 1.5 T[14] with similar volumes and acquisition times, though direct

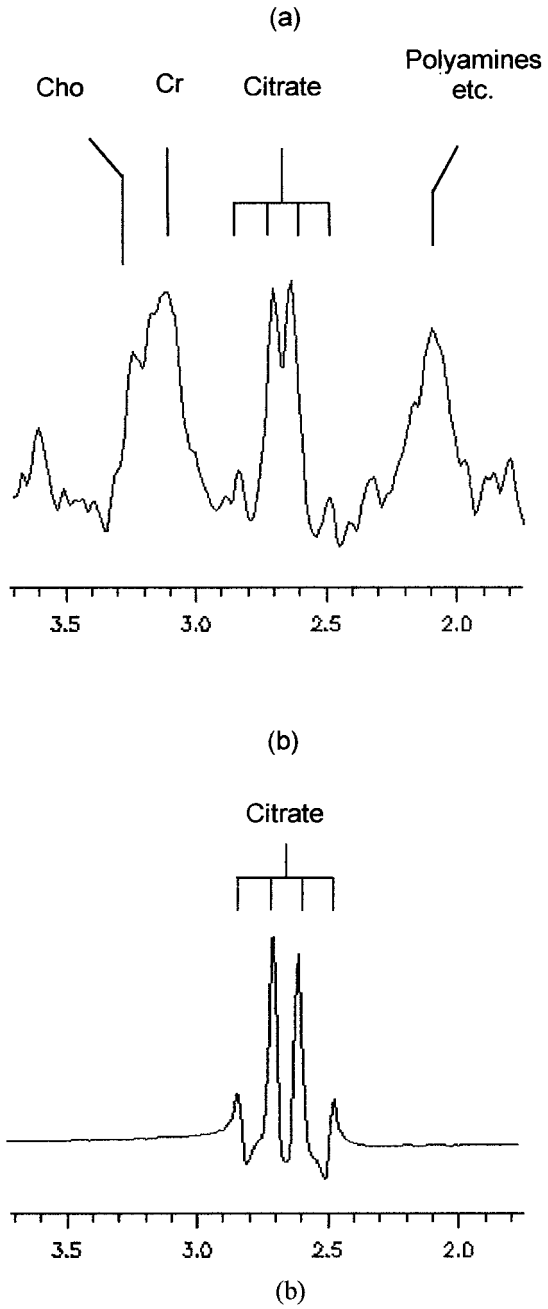

FIGURE 7. a, A STEAM proton spectrum obtained from a 4.5-mL voxel in the central gland of a 60-year-old volunteer (TE = 20 milliseconds, TM = 13.7 milliseconds, TR = 1 second, 512 scans). Four peaks from the strongly coupled methylene in the citrate molecule correspond well to the spectrum obtained from the citrate phantom using the same technique and shown in b.

comparison is again difficult. Four peaks from the strongly coupled methylene protons in citrate molecules are clearly observed in vivo because of the enhanced spectral resolution available at 3 T. Multiplets have been seen previously using 2D J-resolved spectroscopy.[28] The observation of the quadruplet nature can be useful to investigate signal modulation effect of the citrate in vivo in which zero-quantum coherences are present during the mixing time of STEAM sequence.[29] Because there is a significant change observed in chemical shift (δ) and chemical shift between coupled peaks (Δ) versus pH over the physiological range (6.8–7.4), the observation of these 4 peaks could be used as a noninvasive pH monitor for in vivo studies.[30]

In summary, it has been demonstrated that prostate studies on a 3 T whole body MR system are feasible using a TPPA coil when combined with a properly designed T/R switch. Although direct comparison is difficult, it has been demonstrated from a practical standpoint that the SNR in the prostate obtained with the TPPA is comparable or better than the SNR obtained using a PPA at 1.5 T. Although further studies are required for a more accurate comparison using equivalent coil geometries and accounting for relaxation time and prescanning protocol differences, the results are encouraging that prostate studies at high fields will be effective. Furthermore, high quality spectra capable of resolving all 4 proton peaks of the citrate resonance can be obtained. The increased SNR available at 3 T may facilitate practical prostate examinations without the need for an ER coil when the ER coil is contraindicated. It is anticipated that these encouraging results will help drive further studies assessing the utility of high-field MR in areas other than the brain.

ACKNOWLEDGMENTS

The authors thank Dr. J. Ray Ballinger for reading images and Dr. Narayan for his support and consultation. This work was supported by the University of Florida McKnight Brain Institute, the National High Magnetic Field Laboratory, and grant funding from the NIH (R01 DK51014, R01NS41094-01 and P41 RR16105).

REFERENCES

1. Thomas MA, Narayan P, Kurhanewicz J, et al. 1H MR spectroscopy of normal and malignant human prostates in vivo. *J Magn Reson*. 1990; 87:610–619.
2. Kurhanewicz J, MacDonald JM, Vigneron DB, et al. Citrate as an in vivo marker to discriminate prostate cancer from benign prostatic hyperplasia and normal prostate peripheral zone: Detection via localized proton spectroscopy. *J Urol*. 1995;45:459–466.
3. Costello LC, Franklin RB, Narayan P. Citrate in the diagnosis of prostate cancer. *Prostate*. 1999;38:237–245.
4. Maio A, Rifkin MD. Magnetic resonance imaging of prostate cancer: update. *Top Magn Reson Imaging*. 1995;7:54–68.
5. Kaplan I, Oldenburg NE, Meskell P, et al. Real time MRI-ultrasound image guided stereotactic prostate biopsy. *Magn Reson Imaging*. 2002; 20:295–299.
6. Krempien RC, Schubert K, Zierhut D, et al. Open low-field magnetic resonance imaging in radiation therapy treatment planning. *Int J Radiat Oncol Biol Phys*. 2002;53:1350–1360.
7. Coakley FV, Kurhanewicz J, Lu Y, et al. Prostate cancer tumor volume:

measurement with endorectal MR and MR spectroscopic imaging. *Radiology*. 2002;223:91–97.
8. Cruz M, Tsuda K, Narumi Y, et al. Characterization of low-intensity lesions in the peripheral zone of prostate on pre-biopsy endorectal coil MR imaging. *Eur Radiol*. 2002;12:357–365.
9. Bydder M, Larkman DJ, Hajnal JV. Combination of signals from array coils using image-based estimation of coil sensitivity profiles. *Magn Reson Med*. 2002;47:539–548.
10. Ikonen S, Karkkainen P, Kivisaari L, et al. Endorectal magnetic resonance imaging of prostatic cancer: Comparison between fat-suppressed T_2-weighted fast spin echo and three-dimensional dual-echo, steady-state sequences. *Eur Radiol*. 2001;11:236–241.
11. Vilanova JC, Comet J, Capdevila A, et al. The value of endorectal MR imaging to predict positive biopsies in clinically intermediate-risk prostate cancer patients. *Eur Radiol*. 2001;11:229–235.
12. Sugimura K. Staging and tissue characterization of prostate carcinoma: Role of endorectal MR imaging and MR spectroscopy. *Hinyokika Kiyo*. 2000;46:855–859.
13. Narayan P, Kurhanewicz J. Magnetic resonance spectroscopy in prostate disease: Diagnostic possibilities and future developments. *Prostate Suppl*. 1992;4:43.
14. Lowry M, Liney GP, Turnbull LW, et al. Quantification of citrate concentration in the prostate by proton magnetic resonance spectroscopy: Zonal and age-related differences. *Magn Reson Med*. 1996;36:352.
15. Heerschap A, Jager GJ, van der Graaf M, et al. In vivo proton MR spectroscopy reveals altered metabolite content in malignant prostate tissue. *Anticancer Res*. 1997;17(3A):1455–1460.
16. Yue K, Marumoto A, Binesh N, et al. 2D JPRESS of human prostates using an endorectal receiver coil. *Magn Reson Med*. 2002;47:1059–1064.
17. Kurhanewicz J, Vigneron DB, Hricak H, et al. Three-dimensional H-1 MR spectroscopic imaging of the in situ human prostate with high (0. 24–0. 7 cm^3) spatial resolution. *Radiology*. 1996;198:795–805.
18. Kurhanewicz J, Dahiya R, Macdonald JM, et al. Citrate alteration in primary and metastatic human prostatic adenocarcinomas: ^{1}H magnetic resonance spectroscopy and biochemical study. *Magn Reson Med*. 1993; 29:149–157.
19. Straubinger K, Schick F, Lutz O. Relaxation of AB spin systems in stimulated-echo spectroscopy. *J Magn Reson B*. 1995;109:251–258.
20. Bomsdorf H, Helzel T, Kunz D, et al. Spectroscopy and imaging with a 4 Tesla whole-body MR system. *NMR Biomed*. 1988;1:151–158.
21. Chen CN, Hoult DI, Sank J. Quadrature detection coils: A further $\sqrt{2}$ improvement in sensitivity. *J Magn Reson*. 1983;54:324–327.
22. Roemer PB, Edelstein WA, Hayes CE, et al. The NMR phased array. *Magn Reson Med*. 1990;16:192–225.
23. Link J. The design of resonator probes with homogeneous radiofrequency fields. In: Diehl P, Fluck E, Guether H, et al., eds. *In-Vivo Magnetic Resonance Spectroscopy I: Probeheads and Radiofrequency Pulses, Spectrum Analysis*. Berlin: Springer-Verlag; 1992:3–31.
24. Frahm J, Bruhn H, Gyngell ML, et al. Localized high-resolution proton NMR spectroscopy using stimulated echoes: Initial applications to human brain in vivo. *Magn Reson Med*. 1989;9:79–93.
25. Kim JK, Kim DY, Lee YH, et al. In vivo differential diagnosis of prostate cancer and benign prostatic hyperplasia: Localized proton magnetic resonance spectroscopy using external-body surface coil. *Magn Reson Imaging*. 1998;16:1281–1288.
26. Liney GP, Lowry M, Turnbull LW, et al. Proton MR T_2 maps correlate with the citrate concentration in the prostate. *NMR Biomed*. 1996;9:59–64.
27. Bosch CS, Ackerman JH. Surface coil spectroscopy. In: Diehl P, Fluck E, Guether H, et el. eds. *In-Vivo Magnetic Resonance Spectroscopy II: Localization and Spectral Editing*. Berlin: Springer-Verlag; 1992:3–44.
28. Yue K, Marumoto A, Binesh N, et al. 2D JPRESS of human prostates using an endorectal receiver coil. *Magn Reson Med*. 2002;47:1059–1064.
29. Kingsley PB. Scalar coupling and zero-quantum coherence relaxation in STEAM: Implications for spectral editing of lactate. *Magn Reson Med*. 1994;31:315–319.
30. Moore GJ, Sillerud LO. The pH dependence of chemical shift and spin-spin coupling for citrate. *J Magn Reson B*. 1994;103:87–88.